International Journal of Fatigue 184 (2024) 108298

Contents lists available at ScienceDirect

International Journal of Fatigue

journal homepage: www.elsevier.com/locate/ijfatigue

A fatigue life model accounting for the combined effect of surface roughness and microstructure: Application to SLM fabricated Hastelloy-X

Chandrashekhar M. Pilgar [b,d,e], Ana M. Fernandez [c], Javier Segurado [b,a,*]

[a] IMDEA Materials Institute, C/Eric Kandel 2, 28906 Getafe, Madrid, Spain
[b] Department of Materials Science, Universidad Politécnica de Madrid E.T.S. de Ingenieros de Caminos, 28040 Madrid, Spain
[c] Industria de Turbo Propulsores, Department of Materials and Processes, ITP Aero SAU, Zamudio, 48170, Bizkaia, Spain
[d] Sanjivani College of Engineering Kopargaon, 423603, Maharashtra, India
[e] Mines Paris, PSL University, Centre for material forming (CEMEF), UMR CNRS, 06904, Sophia Antipolis, France

ARTICLE INFO

Keywords:
Hastelloy-X
Surface roughness
Microstructure sensitive fatigue
Crystal plasticity
FFT based homogenization

ABSTRACT

This study introduces a microstructure-sensitive fatigue life prediction framework based on CP-FFT which includes the effect of surface roughness. The model is applied to flat Hastelloy-X specimens fabricated using Selective Laser Melting. The surface roughness measured is incorporated introducing a free surface with sinusoidal profile. The framework can accurately predict the fatigue life reduction of rough flat specimens using the fatigue parameters of polished bulk specimens and introducing the actual microstructure and roughness. A parametric study shows a monotonic reduction of life with the roughness amplitude but a minor effect of the surface waviness.

1. Introduction

Selective laser melting (SLM) is an additive manufacturing process which aims at producing near net shaped metallic components. However, the fatigue performance of these parts is usually lower than that of their wrought counterparts. This reduction in the performance is due to the combined effect of several features consequence of the fabrication process including porosity, residual stresses, surface roughness and strong texture.

Among these factors, porosity and residual stresses are less critical, because they can in general be released by a combination of optimization of the SLM process parameters and post fabrication treatments [1]. On the other hand, *surface roughness* is probably the most influential microstructural feature in the fatigue life and the processes designed to minimize its influence are usually incompatible with the dimensional tolerances required for an engineering part. The surface roughness in SLM fabricated parts has different origins including the stair-step effect, the presence of partially melted powder particles on the final part surface, and the Plateau–Rayleigh instability [2]. The mechanical effect of this roughness is the presence of small stress concentrations along the irregular surface which act as fatigue crack initiation sites, strongly reducing the fatigue performance of the fabricated part. Numerous researchers have explored the effect of surface roughness on the fatigue behavior of SLM parts, as well as potential mitigation methods. Ferrar et al. [3] and Ali et al. [4] have highlighted the low repeatability of fatigue tests due to surface roughness, resulting in a random distribution of defects. Mumtaz and Hopkinson [5] observed that decreasing the laser scan speed could reduce the roughness of the top surface while increasing the roughness of the side surface in IN625. Similarly, Esmaeilizadeh et al. [6] reported a reduction in surface roughness by lowering the laser scan speed, in the case of Hastelloy-X. Abele and Kniepkamp [7] demonstrated that the use of a contour scan method could significantly reduce surface roughness. Wang et al. [8] found that remelting the surface layers could minimize the surface roughness of SLM Hastelloy-X. Despite of all these efforts, none of the aforementioned approaches can entirely eliminate the surface roughness.

Due to the strong influence of the surface roughness in the fatigue performance and the difficulty of eliminating it, it becomes essential to understand and quantify the effect of the surface condition on the fatigue life. This need also extends to cases involving contact and wear [9,10], where the effect of roughness is also remarkable.

In the case of uniaxial fatigue, the analysis of the effect of the surface condition requires tests on specimens with controlled surface roughness and the development fatigue models which consider the rugosity and its combined effect with other microstructural features, such as texture or grain shape, to quantify its influence on fatigue life.

Early attempts to model the influence of surface roughness were based on linear elastic fracture mechanics (LEFM), with all micro-notches assumed to be micro-cracks and designs based on the material fatigue crack propagation threshold ΔK_{th} [11,12]. These ap-

* Corresponding author at: Department of Materials Science, Universidad Politécnica de Madrid E.T.S. de Ingenieros de Caminos, 28040 Madrid, Spain.
E-mail address: javier.segurado@upm.es (J. Segurado).

https://doi.org/10.1016/j.ijfatigue.2024.108298
Received 7 December 2023; Received in revised form 19 March 2024; Accepted 21 March 2024
Available online 27 March 2024

proaches are macroscopic, assume elastic fracture mechanics and may be overly conservative. Several empirical models, such as the Murakami method [13], were developed by connecting fatigue strength to defect size and micronotches. Subsequently, Pessard et al. [14] and Le et al. [15] developed stochastic models based on the LEFM and Dang Van criteria. These models were able to quantify the effect of surface roughness on fatigue life reduction; however, they were mainly empirical and macroscopic, without taking into account microstructural characteristics or surface roughness topology.

The quantification of surface roughness is essential when modeling the effects of surface roughness, and modern technology allows for highly accurate surface topography (down to the sub-micrometer level) to be produced through contact and non-contact profilometry. This topological description can be incorporated into computational models. Campbell et al. [16] used trigonometric equations to include surface roughness caused by the staircase effect in CAD files. Pérez et al. [17] developed a model based on sample and defect geometry that takes into account the average surface roughness, R_a. These articles focus on empirical descriptions of surface roughness in bulk samples and do not directly address its impact on fatigue performance. Surface topography can be used as an input for crystal plasticity finite element models (CPFE) to take into account the effect of surface roughness on fatigue performance. As reported by As et al. [18], this approach was used to predict fatigue in an aluminum alloy, with average surface roughness R_a as the roughness descriptor. Subsequently, Bezier spline interpolation formulas were used in FE models to replicate surface roughness profiles [19]. Yadollahi et al. [20] accurately estimated the fatigue life of IN718 by constructing a surface roughness profile based on a semicircular locus whose dimensions were determined by the maximum depth of the valley. Vayssette et al. [21] provided the most promising methodology to date that directly incorporated experimental 3D profilometry measurements into an FE model of the specimen to statistically study fatigue performance. All these models provide some interesting insights to the quantification of surface roughness and its effect in the fatigue performance, but do not consider the polycrystalline microstructure which influence in the nucleation of fatigue cracks is critical.

Very few works can be found in the literature which explore the combined effect of surface roughness and polycrystalline microstructure. One of the first works was published by Belhadjamor et al. [22], who proposed a CPFE methodology with random sinusoidal Gaussian surface profiles and optimized them with skewness and kurtosis fitting based on experimental observations. However, the application of the model to predict fatigue life was not explored. The most relevant work studying the synergistic effect of surface roughness and microstructure in fatigue life was proposed recently by Natkowski et al. [23] for wrought steel, based on Bashkin equation and Fatigue Indicator Parameters extracted from CPFE calculations.

There are several features that are not considered in the studies mentioned. First, all the studies including macroscopic and CPFE based ones, are focus on bulk (thick) samples. However, in the case of thin samples the surface roughness effect is even amplified because of the additional factor of the varying cross section, which can cause stress concentration in certain areas. Moreover, on flat samples, the surface effect is added to the higher anisotropy in the mechanical response caused by the microstructures formed by the high temperature gradients during fabrication, and the effect of surface roughness varies depending on the fabrication direction. Second, to the authors knowledge, the few papers modeling surface roughness are focused on other metals with very different casuistic, such as steels [23]. Third, no work can be found that parametrically study the different descriptors of surface roughness surface such as waviness and intrusion depth. Finally, the available models do not provide any statistical description of the fatigue life but are just based on individual simulations, probably due to the high cost of CPFE simulations.

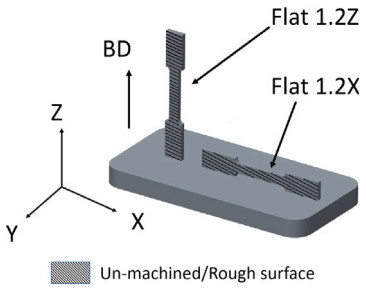

Fig. 1. Description of coupon of flat sample with 1.2 mm thickness built in Z and X direction. The rough or un-machined surfaces are marked with textured lines.

In this paper, the fatigue life prediction framework developed in Pilgar et al. [24] for bulk Hastelloy-X is extended to account also for the effect of surface roughness. As the original framework, the fatigue life statistical prediction is based on the solution of a set Statistically Representative Volume Elements solved using CPFFT, but including in the models a free surface with a harmonic description of surface roughness. To validate the model, new fatigue experiments are performed for plane SLM specimens of Hastelloy-X with two surfaces containing as-built roughness, and the data obtained in the experimental characterization of these surfaces is used to build the model. Then, a parametric study will be performed to analyze the effect of surface roughness amplitude and waviness on the fatigue performance

2. Fabrication and experimental characterization

Hastelloy-X flat specimens of 1.2 mm thickness were fabricated using a SLM technique in a RenAM 500Q machine. Resulting specimens were machined as rectangular dog bone shapes with a gauge length of 15.68 μm. Two type of samples were built with orientations parallel to the building direction (flat 1.2Z) and perpendicular to the build direction (flat 1.2X) (Fig. 1). After fabrication, all samples were heat treated at 1170 °C for 30 min and then quenched with a gas fan. The samples were tested in an annealed condition.

The flat samples fabricated by SLM have surface roughness as a result of the presence of partially melted and unmelted powder. The XZ section is left in its original state because it is difficult to machine due to geometric complexities and therefore presents surface roughness. On the contrary, the other surfaces of the samples are machined and the surface roughness is eliminated in these faces. Fig. 1 presents a schematic of the two fabricated samples indicating their orientation with respect fabrication and showing the rough surfaces.

To measure the surface roughness of the XZ surfaces of the flat specimens, the profilometer "Mitutoyo SJ-210" with a stylus is used in accordance with the ISO-4287 standard. The surface roughness is represented by arithmetic mean surface roughness R_a, which is measured over a length as,

$$R_a = \frac{1}{L}\int_0^L |y| dz \tag{1}$$

where y represents the deviation from the average y-position of that surface. It is important to note that the surface roughness in Eq. (1) is in the Y direction. The resulting mean surface roughness value obtained was $R_a \approx 10$ μm. In addition, an average wave length of 60 μm is measured from profilometry.

In flat samples a complex microstructure is formed near the free surface, characterized by columnar grains elongated along the Y-axis, termed the "border" and which typically spans approximately 0.2 mm width for each free surface, corresponding to 1–2 grains [25]. In the building direction of flat samples, grains are elongated with an average aspect ratio of 10:1 for 1.2 mm samples. A flat sample of this thickness

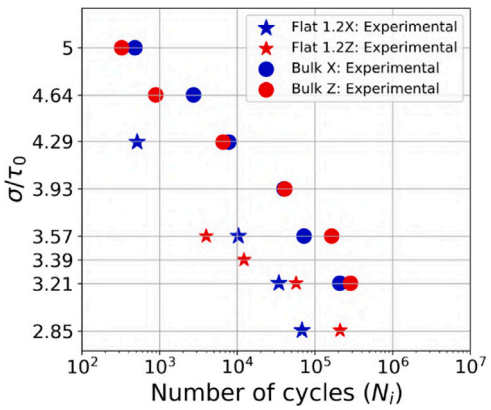

Fig. 2. The experimental stress-life curve for flat 1.2X, 1.2Z sample along with bulk samples built in X and Z direction.

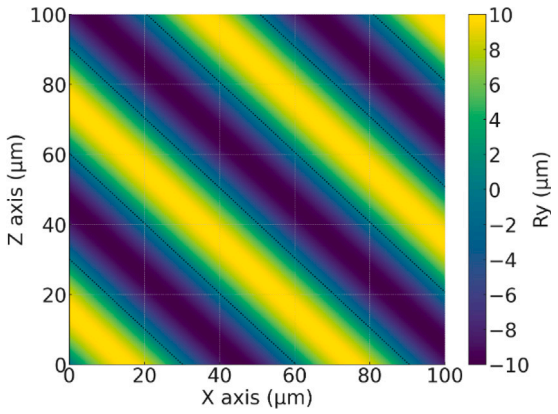

Fig. 3. The graphical representation of the surface roughness profile showing XZ section.

typically contains 4–5 grains along the Y direction, having preferential orientations, which leads to a notably anisotropic material response.

The uniaxial cyclic behavior of SLM-fabricated Hastelloy-X at 750 °C was experimentally determined by conducting cyclic tests with a wide range of stress amplitudes. The flat sample oriented in the Z direction (flat 1.2Z) was subjected to uniaxial stress-controlled cyclic loading in the building direction (Z), while the sample oriented in the X direction (flat 1.2X) was subjected to uniaxial cyclic loading in the X-direction. The cyclic tests for stress-controlled loading were carried out with $\frac{\sigma}{\tau_0}$= 2.85,3.21,3.39,3.57 and $\frac{\sigma}{\tau_0}$= 2.85,3.21,3.57,4.29 for flat 1.2Z and flat 1.2X samples respectively, with a stress ratio of R_σ=0.03. τ_0 is a normalization factor, corresponding to the critical resolved shear stress of Hastelloy-X grains at 750 °C, which was used due to the confidentiality agreement signed with the industrial partner that funded this study.

The resulting fatigue life (number of cycles N) as function of the applied stress range (σ) under stress control is shown on Fig. 2. For comparison, the corresponding S-N results obtained for bulk samples (constructed in X and Z directions) with ultrafine surface polishing (with $R_a \leq 0.2$ μm) under the same testing conditions, taken from Pilgar et al. [24], are also included.

The results presented in Fig. 2 show a clear decrease in life for the flat samples compared to the bulk ones. It is found that, for low applied stress ranges, the samples built in the X orientation are slightly more resistant to fatigue than the ones fabricated the Z direction (see Fig. 2), similar to what is observed in bulk samples [24] and in agreement with literature results [8,26]. However, fatigue anisotropy cannot be confirmed from an experimental point of view for high stress levels due to the limited experimental data available.

3. Computational homogenization framework

3.1. Representative Volume Element generation

The microstructure of SLM Hastelloy-X is represented using cuboidal Representative Volume Element (RVE) which, as in the works of Pilgar et al. [24,25], statistically reproduce the grain size, shape, and orientations obtained from the EBSD measurements. The microstructure represented in the RVEs is voxelized to be directly used in CPFFT simulations. The method of generating synthetic RVEs, including grain size, aspect ratio, and orientation, is discussed in the aforementioned papers.

The surface roughness of the actual specimens was located on the YZ section of the flat samples. To accurately represent the deformation of the plain samples, the RVEs meet certain criteria:

- RVEs are right rectangular prisms with different edge lengths, being their relative edge lengths equal to the aspect ratio of the grains.
- RVEs include very compliant buffer layers to emulate stress-free boundary conditions in the planes perpendicular to the sample thickness (YZ plane). This free conditions are fundamental to consider the influence of the ratio between the actual specimen thickness and grain size.
- RVEs are considered periodic in the other two directions, because the sample size in those directions is much larger than grain size.
- Surface roughness is introduced in the YZ surfaces as the shape of the buffer region.

Regarding the shape of rough surfaces, a typical observation of the surface roughness profile is that it approximately resembles a sine curve shape [27,28]. Therefore, in this study, surface roughness is expressed by a simplified sinusoidal curve with amplitude R_a and wavelengths λ_x and λ_z in X and Z direction respectively, which is given as,

$$R_Y = R_a\left(\sin\left(\frac{x}{\lambda_x}+\frac{z}{\lambda_z}\right)\right). \quad (2)$$

A graphical representation of the surface roughness shape, defined in Eq. (2), is shown as in Fig. 3.

The average wavelength of surface roughness profiles in the X and Z directions is approximately the same ($\lambda_x \approx \lambda_z$), and its measured value is 60 μm. The buffer layers of the compliant material are placed on top and bottom of the cell in the Y direction and its surface has the shape defined by Eq. (2).

The resulting RVE is represented in Fig. 4. Fig. 4(a) depicts the original periodic RVE that takes into account microstructural features such as grain size, shape, and orientation to represent machined samples. The shape of the buffer surfaces can be observed in Fig. 4(b), left part. Note that the microstructure is periodic on X and Z directions, and periodic boundary conditions are considered on those edges. The approximated number of crystals in the models is around 850, and the discretization of the RVEs was done in 64 × 32 × 128 voxels. The resulting RVE with surface roughness is shown in the right part of Fig. 4(b).

3.2. Crystal plasticity model

It is known that plastic behavior might show an intrinsic size effect which introduces a dependency of the response with some internal characteristic length. The characteristic length of the microstructure influencing the response is normally the grain size [29], but for non-smooth free surfaces, the characteristic length might be related with the roughness depth or spatial frequency. Indeed, the critical role of

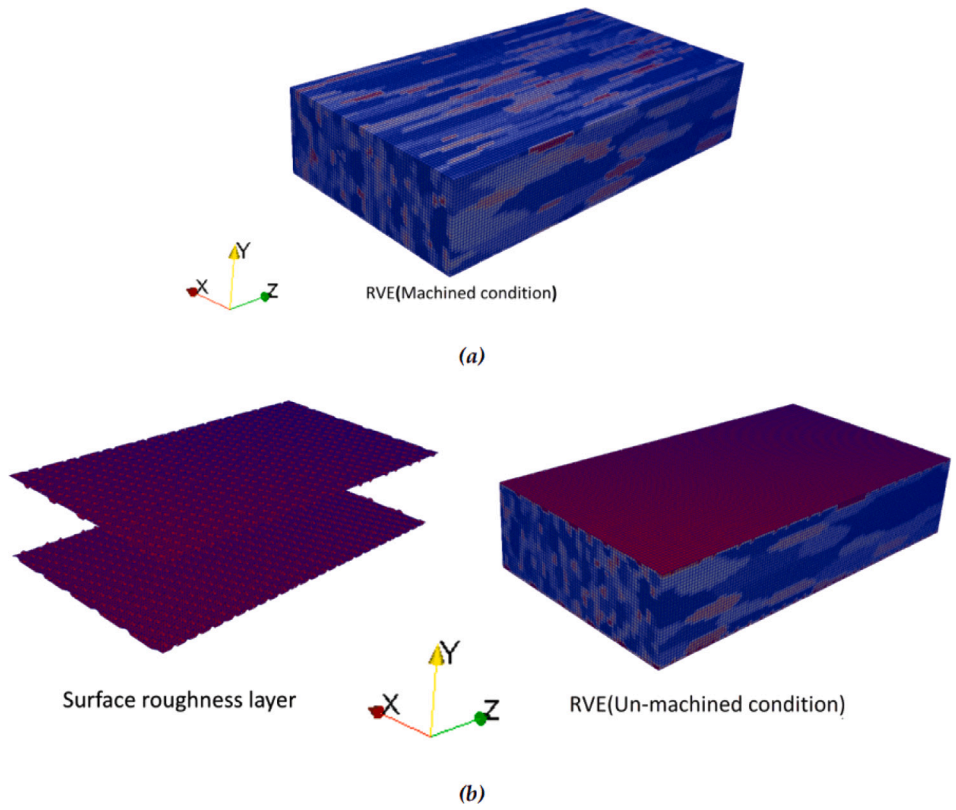

Fig. 4. 3D non cubic RVEs of polycrystalline SLM Hastelloy-X for flat sample 1.2X in (a)machined and (b, right) as-built(with surface roughness) condition. (b, bottom) shows the layer of surface roughness. Note that the colors indicate the grain numbers.

the characteristic lengths of the surface waviness has been observed in tribological studies [9] and has been rationalized by discrete dislocation dynamics (DDD) simulations [30]. However, a DDD framework is non feasible for studying large three dimensional polycrystals and crystal plasticity is chosen here. Moreover, although this size effect could be captured by strain gradient CP models [29] or micromorphic approaches [31], these models are still too expensive to allow considering multiple realistic 3D RVEs for the statistical description required in fatigue. Therefore, a standard phenomenological crystal plasticity (CP) model is used to simulate the elasto-viscoplastic cyclic behavior of Hastelloy-X. The model incorporates essential aspects such as isotropic and kinematic hardening, as well as mean stress relaxation effects [32]. A detailed description of the crystal plasticity model can be found in our previous publication [24], and here only a concise summary is provided for completeness.

The plastic slip rate $\dot{\gamma}^{\alpha}$ in each slip system α is defined by a power law, which is given as

$$\dot{\gamma}^{\alpha} = \dot{\gamma}_0 \left(\frac{|\tau^{\alpha} - \chi^{\alpha}|}{g^{\alpha}} \right)^{\frac{1}{m}} \text{sign}(\tau^{\alpha} - \chi^{\alpha}) \tag{3}$$

where τ^{α}, χ^{α} and g^{α} correspond to the resolved shear stress, back-stress and the critical resolved shear stress on the slip system α respectively. γ^0 and m are the reference strain rate and the strain rate sensitivity parameters.

The plastic flow follows a CP extension of Ohno-Wang model considering only the first two terms [32],

$$\dot{\chi}^{\alpha} = c\dot{\gamma}^{\alpha} - d\chi^{\alpha}|\dot{\gamma}^{\alpha}| \left(\frac{|\chi^{\alpha}|}{c/d} \right)^{k} \tag{4}$$

The c, d, and k are material parameters, with k controlling the mean stress relaxation, and c and d representing the direct hardening and dynamic recovery modulus, respectively. The evolution of the Critical Resolved Shear Stress (CRSS) for a given slip system, g^{α}, determines the isotropic hardening and is expressed as

$$\dot{g}^{\alpha} = \sum_{\beta} q_{\alpha\beta} h(\gamma_a) |\dot{\gamma}^{\beta}| \tag{5}$$

where $q_{\alpha\beta}$ are the latent hardening coefficients and h is the self hardening modulus which follows the Voce hardening model [33], given by

$$h(\gamma_a) = h_s + \left[h_0 - h_s + \frac{h_0 h_s \gamma_a}{\tau_s - \tau_0} \right] exp^{\left(\frac{-h_0 \gamma_a}{\tau_s - \tau_0} \right)}. \tag{6}$$

In the hardening equation τ_0, τ_s, h_0 and h_s are the hardening parameters and γ_a is the accumulated plastic shear.

The FFT based homogenization code FFTMAD [34,35] was used to simulate the cyclic plastic response. The Galerkin-FFT algorithm was chosen to solve the homogenization problem [36] in a finite deformation set [37], using Newton–Raphson and the conjugate gradient method for solving the linearized equations. Modified frequencies were introduced to alleviate noise [38]. The incorporation of external macroscopic loading, which is prescribed by setting a combination of the macroscopic deformation gradient and the first components of the Piola stress, into the FFT problem was achieved using the mixed control technique developed by Lucarini and Segurado [39]. The macroscopic stress was applied in cycles representing the experimental loading and each cycle was discretized in increments.

4. Results

4.1. Simulation set-up

The crystal plasticity model parameters used are taken from Pilgar et al. [24] and given in Table 1. These parameters were obtained from the inverse analysis of cyclic tests of bulk AM Hastelloy-X specimens. Nevertheless, the same crystal response is assumed here for plane

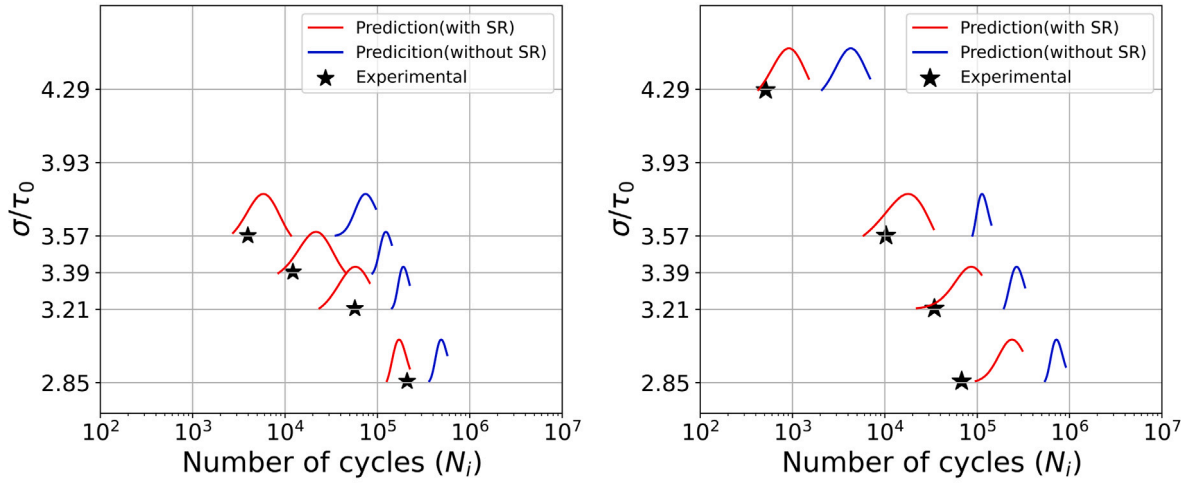

Fig. 5. Comparison between predicted and experimental fatigue life(shown by black asterisk) under machined(without surface roughness, SR) represented by blue lines and un-machined(with SR) conditions, shown by red lines for (a) flat 1.2Z and (b) flat 1.2X samples.

Table 1
Crystal plasticity parameters of a SLM Hastelloy-X at 750 °C [24].

Elastic (GPa)	C_{11}	C_{12}	C_{44}	
	194.8	126.91	89.95	
Viscoplastic	m	$\dot{\gamma}_0$ (s^{-1})		
	0.017	2.42×10^{-3}		
Isotropic Hardening (MPa)	τ_0	τ_s	h_0	h_s
	τ_0	$1.25\tau_0$	$78.7\tau_0$	$0.71\tau_0$
Kinematic Hardening	c (MPa)	d	k	
	$171.42\tau_0$	$2.57\tau_0$	0.1066	

specimens, following the conclusions of Pilgar et al. [24,25] where it was shown that the variations in mechanical response observed when changing the direction of the building or the shape of the sample were solely attributable to changes in microstructure.

Microstructure-sensitive models aim at correlating the microstructure and the fatigue performance of an alloy by studying the cyclic plastic deformation of a RVE of the microstructure resolving both macroscopic response and microfields [40–42]. The RVEs include microstructural characteristics like grain size, shape, and orientation. The microfields obtained in the simulations are used to define the driving forces for crack formation through the definition of microscopic fatigue indicator parameters (FIP) which correlate with fatigue life [42]. Several FIPs are proposed in the literature, including accumulated plastic slip per cycle [40,43–45], Fatemi-Socie parameter [46,47], energy stored per cycle [44,48,49], energy dissipated per cycle [50], and others [51,52]. There is no universally valid FIP, and its choice depends on the particular alloy (e.g. presence of twin bands as hotspots) or on a particular fatigue regime (e.g. FIPs including elasticity can be used for HCF [53]). Finding the most appropriate FIP is usually made based on experience or on trial and error, nevertheless even machine learning techniques have been used to find the optimal FIP that links simulation and experimental results [54]. In the absence of dedicated experiments to find the optimal FIP, a clever choice is the use of FIPs having a physical background. For cyclic tests involving plastic deformation, initiation criteria based on the total energy stored before fracture [48] or on the total dissipated energy [50,55] are common and have shown a very good predictive capacity since they encompass both plastic strain and stress levels. In this study, among the physically based FIPs, the plastic work dissipated per cycle has been chosen since it has provided good predictive capacity for stress controlled tests in Hastelloy-X [24]. In particular life is predicted based on the maximum value of this FIP in a band before the elastic shakedown for all the SVE, W_p^{acc}, as introduced in the previous work [24].

A power-law expression is proposed to link fatigue life (number of cycles N_i) and FIP,

$$N_i = \frac{W_\sigma^{crit}}{(W_p^{acc})^{nk}}, \tag{7}$$

in which W_σ^{crit}, and nk are the two fitting parameters characterizing the alloy fatigue performance. These constants were obtained in Pilgar et al. [24] for a SLM bulk sample. No fitting at all has been done to calibrate the fatigue law parameter to the flat sample experiments, and the same law and parameters proposed for bulk specimens are used here. The reason for using the same parameters is the hypothesis that the material has the same composition and sub-grain structure for the bulk and flat specimens and differences in fatigue life can be attributed and modeled only by considering the microstructure and roughness changes. Therefore, the parameters of the fatigue life prediction model (Eq. (7)) taken from Pilgar et al. [24] are ${W_{crit}}^{\sigma} = 5.06 \times 10^8$ and $nk = 0.56$.

To compare the effect of free non-smooth surfaces to flat smooth specimens, two sets of simulations are conducted. The first set involves a statistically representative volume element (SVE) of 20 randomly generated microstructures that represent perfectly periodic flat specimens without any surface effects. These models reproduce the average grain size, aspect ratio, and grain orientations observed in flat 1.2X and flat 1.2Z samples and are referred to as "machined" specimens.

The second set of simulations involves another 20 RVEs comprising different microstructures that correspond to the models depicted in Fig. 4b, which introduce surface roughness on the lateral planes perpendicular to the thickness of the sample, while the other two directions remain fully periodic. These models reproduce the average grain size, aspect ratio, and grain orientations observed in plain 1.2 mm samples, and include a variable level of porosity characterized by the parameters R_a and λ_x, λ_y. These specimens are referred to as "as-built" samples.

4.2. Effect of surface roughness: comparison with the experiments

The SVEs underwent virtual uniaxial stress-controlled cyclic tests for all the stress ranges experimentally tested and under a stress ratio of $R_\sigma = 0.03$ for both the machined and as-built conditions. The SVEs of "as-built" materials included a free rough surface described with Eq. (2) using the values found experimentally with profilometry, $R_a \approx 10$ μm and $\lambda_x = \lambda_y \approx 60$ μm.

Cumulative FIPs, W_p^{acc}, were determined from the results of each of the 20 different RVEs simulated for each condition. This ensemble of RVEs forms a large-scale statistical volume element (SVE) which provides a statistical distribution of fatigue life that characterizes a given microstructure and loading condition.

The fatigue crack initiation life of the flat samples 1.2Z and 1.2X is depicted in Figs. 5(a) and 5(b), respectively. The curves represent the probability distribution function of fatigue life for the stress level marked as a horizontal line and labeled on the vertical axis. The probability distribution functions shown are the adjustment of the results of all the different RVEs for that loading case to a log-normal distribution. Two colors are used for the distributions, blue corresponds to the predicted life probability distribution without surface roughness, while the red lines indicate the predicted life in "as-built" condition (with surface roughness). The corresponding experimental life is represented by black asterisks. Note that surface roughness is abbreviated as SR in the figure. For both orientations the agreement between the fatigue life predicted numerically and the experimental results when surface roughness is taken into account is remarkable. The largest differences were observed for the flat 1.2X sample in the stress ranges σ/τ_0, 2.85, and 3.21, where the fatigue life is somewhat overestimated. On the contrary, if surface roughness is not introduced in the model and standard periodic boundary conditions are used, the microstructure and shape of the sample will be the only factors controlling fatigue cracks initiation. In Figs. 5(a) and 5(b), the fatigue life prediction without considering surface roughness is represented by blue lines for samples 1.2Z and 1.2X, respectively. It is evident that in this case the predicted life is highly overestimated. Therefore, for flat samples with considerable surface roughness, microstructure alone is not enough to predict fatigue life, and it is essential to include free surfaces with roughness into account when modeling.

The results of this section demonstrate that the model is capable of accurately predicting fatigue life taking into consideration the effects of microstructure, surface roughness, and shape of the samples. It is notable that the predicted fatigue lives for both flat samples are in agreement with the experimental results, considering that the fatigue life law used for the predictions was only calibrated using two experiments of Bulk-X samples (see Pilgar et al. [24]) well polished.

Regarding the statistical dispersion of the fatigue life, it is widely accepted that as the cyclic stresses applied are reduced the variation in fatigue live increases. However, it can be observed in Figs. 5(a) and 5(b) that it is not the case for the simulation of these SLM fabricated flat samples. Here the variability remains high also for high stress amplitudes because the number of grains is relatively small compared to a macroscopic specimen, and the different samples statistically equivalent have a slightly different plastic response.

Effect of building orientation

The S-N curves in Fig. 6 show the impact of the building direction on the fatigue life of flat samples, taking into account surface roughness. The horizontally built sample (flat 1.2X) shows greater resistance to the initiation of fatigue cracks than the vertical sample (flat 1.2Z) for high to medium stresses. In the case of low stresses, experimental data show a change in the tendency, (Fig. 6. Due to the limited experimental data at low stresses it cannot be stated if this change of tendency, neither observed in other experimental work nor in the simulations, is a characteristic of the material or is just the result of a particular test.

The proposed CP-FFT model is able to reproduce the fatigue anisotropy for medium to high stress, consistently with the research findings of Shrestha et al. [26] and Wang et al. [8]. The model also predicts a progressive reduction of the anisotropy of the fatigue performance with stress range reduction. On the contrary, the model does not accurately predict fatigue life at the two lowest stress levels $\sigma/\tau_0 = 2.85, 3.21$. This difference can be explained by the very long times of the tests at these stresses which enhance the effect of fatigue-creep interaction mechanisms that are not directly considered in the model.

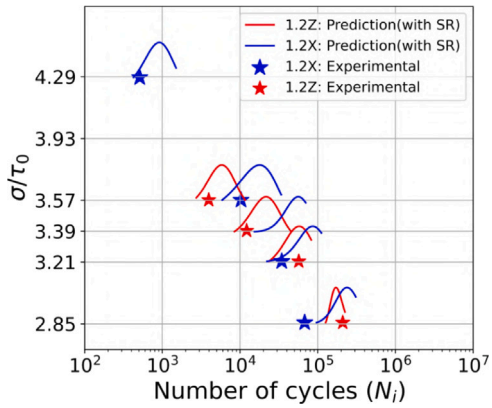

Fig. 6. The comparison between experimental and predicted fatigue lives of flat 1.2X and flat 1.2Z, showing the effect of building orientation on fatigue performance of flat samples.

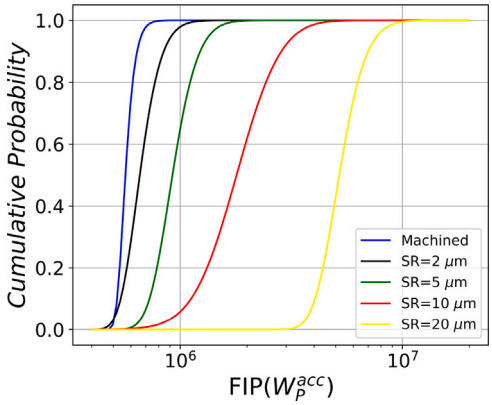

Fig. 7. The fatigue indicating parameters (FIPs) predicted for different amplitudes of surface roughness for the loading case, σ/τ_0=3.57 in 1.2X orientation.

4.3. Parametric study on effect of surface roughness parameters

After the validation of the fatigue life prediction model for the experimental results available and including roughness, in this section, the model will be used to perform a parametric numerical study of the influence of surface roughness on the fatigue life of flat specimens. In the study, both surface roughness amplitude and wavelength will be systematically varied.

4.3.1. Effect of surface roughness amplitude

The mean amplitude of surface roughness in the plane specimens was quantified as $R_1 = 10$ μm (see Section 2) and the models presented in Section 3 included this experimental value in the function defining the surface shape (Eq. (2)). In this section the parameter R_a will be set to five different values, 0μm (perfect smooth machined specimem), 2 μm, 5 μm, 10 μm, and 20 μm of amplitude. The values with less R_a than the experimentally measured are the typical values that can be obtained in Hastelloy-X from electropolishing after SLM [56].

The wavelength of surface roughness was maintained as $\lambda_x = \lambda_y = 60$ μm. For each case, 20 Representative Volume Elements were simulated for both orientations and under various loading conditions. A significant correlation between surface roughness amplitude and FIP was observed, wherein an increase in amplitude led to a corresponding increase in FIP. This trend was consistent across all loading conditions and orientations, showing the pronounced influence of surface roughness amplitude on predicted fatigue behavior. The origin of this effect is the increase of the deviatoric stresses with roughness near the

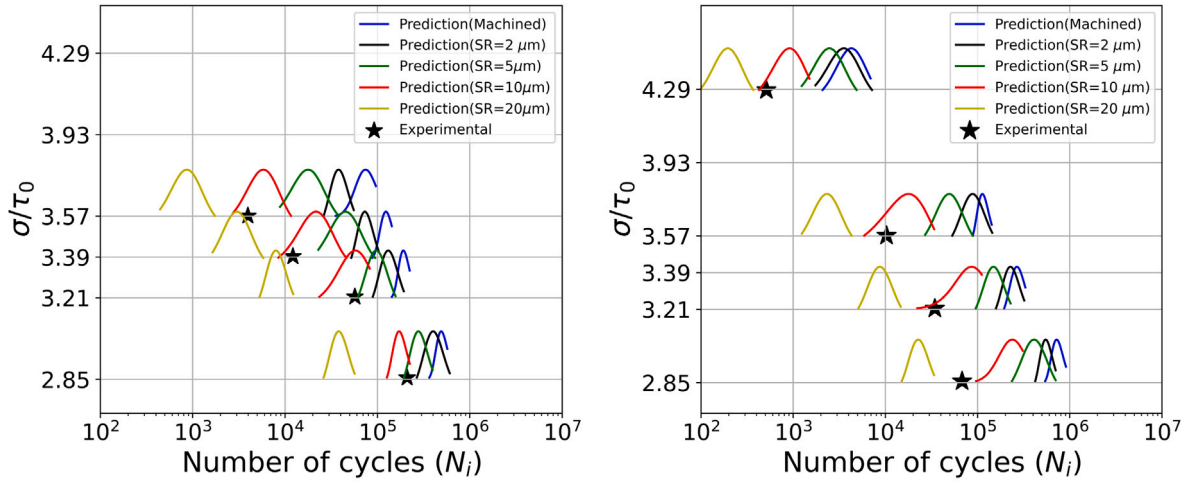

Fig. 8. The comparison of computational fatigue life for different amplitude of surface roughness for (a) flat 1.2Z and (b) flat 1.2X samples. Please note that the black asterisk represents the experimental fatigue life at 10 μm amplitude.

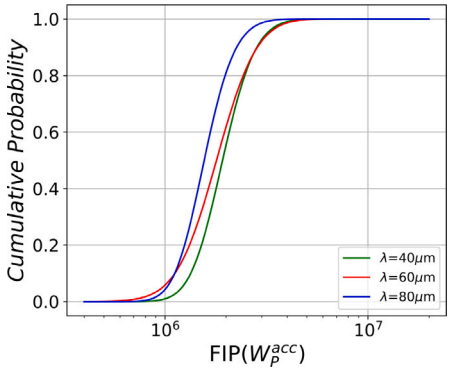

Fig. 9. The fatigue indicating parameters (FIPs) predicted for different wavelengths of surface roughness for the loading case, σ/τ_0=3.57 in 1.2X orientation.

free surface, leading to higher resolved stresses and slip, which finally results in higher values of the dissipated energy per cycle.

To statistically analyze this effect, Fig. 7 represents the FIP Cumulative Distribution Function (CDF) for all the roughness amplitudes considered for a particular loading case, σ/τ_0=3.57, and 1.2X orientation. It is observed that as the roughness amplitude increases, the CDF moves to the right, presenting higher FIP values. At the same time, statistical dispersion also increases with roughness with the exception of the largest depth. This systematic deviation of the CDF to the right is due to the increment of the stress concentration around the notches and will result in a fatigue life reduction for increasing roughness.

Once the FIPs are calculated for each RVE, the fatigue crack initiation of the flat specimens in the two orientations is depicted in Fig. 8. The experimental fatigue life is indicated by the black asterisks. It is observed in the figure that a clear reduction in fatigue life is predicted for increasing amplitudes of the surface roughness layer. It should be remarked that fatigue life prediction model and parameter are kept from Pilgar et al. [24] and the only difference among the results is the roughness depth. The model is therefore sensitive to surface roughness amplitude and qualitatively predicts the experimental trends observed. There are no available results for Hastelloy-X and different roughness, but the ranking of the roughness amplitudes with respect the life reduction reproduced by the model is similar to some experimental studies on other SLM fabricated materials [57].

4.3.2. *Effect of surface roughness wavelength*

The criterion for selecting surface roughness wavelength in the comparison with experiments is the actual layer thickness during the Selective Laser Melting (SLM) process, which is 60 μm, and it was shown that the use of this value and the measured R_a provided accurate predictions of the experiments.

To evaluate the sensitivity of fatigue crack initiation on the surface roughness spatial frequency, different wavelengths were considered: 40 μm, 60 μm (corresponding to the layer thickness), and 80 μm. Wavelengths in both the X and Z directions, λ_x and λ_z are assumed to be identical, as represented in Eq. (2). The surface roughness amplitude was held constant at 10 μm for all cases. For each orientation (1.2Z and 1.2X) and loading condition, twenty RVEs were simulated to analyze the effect of surface roughness wavelength on fatigue behavior.

The numerical analysis shows that minimal dependence on surface roughness wavelength was observed in the cumulative distribution function of the FIP. Fig. 9 illustrates the variation in FIP for different wavelengths under a fix loading case σ/τ_0=3.57 and fabrication direction(X). A small increase in FIP was noted with decreasing wavelength; however, this variation was marginal, particularly in the context of stochastic behavior in fatigue events.

The CDF of FIPs is used to predict fatigue life distributions. Fig. 10a and 10b show numerical predictions of fatigue lives for three different surface roughness wavelengths for both orientations and under various loading conditions. A small increase in fatigue lives was observed with an increase in wavelength. Specifically, the percentage difference between mean fatigue lives for 60 μm and 80μm was found to be less than 4%, while the difference between 60 μm and 40 μm was less than 3.5%. These results suggest a marginal sensitivity of fatigue lives to surface roughness wavelength.

Fatigue crack initiation is a localized phenomenon and typically occurs at sites of stress concentration such as micro-notches or surface irregularities. The depth or amplitude of these notches significantly influences crack initiation, with larger amplitudes facilitating easier crack initiation due to increased stress concentration. Conversely, the influence of surface roughness wavelength on fatigue crack initiation is relatively minor. Although lower wavelengths statistically yield more micro-notches on the surface, crack initiation ultimately occurs from just one (or very few) of these micro-notches. Therefore, while surface roughness wavelength may influence the statistical distribution of micro-notches, its impact on the overall fatigue crack initiation process is limited compared to notch amplitude. The small effect of roughness waviness found also validates the experimental characterization

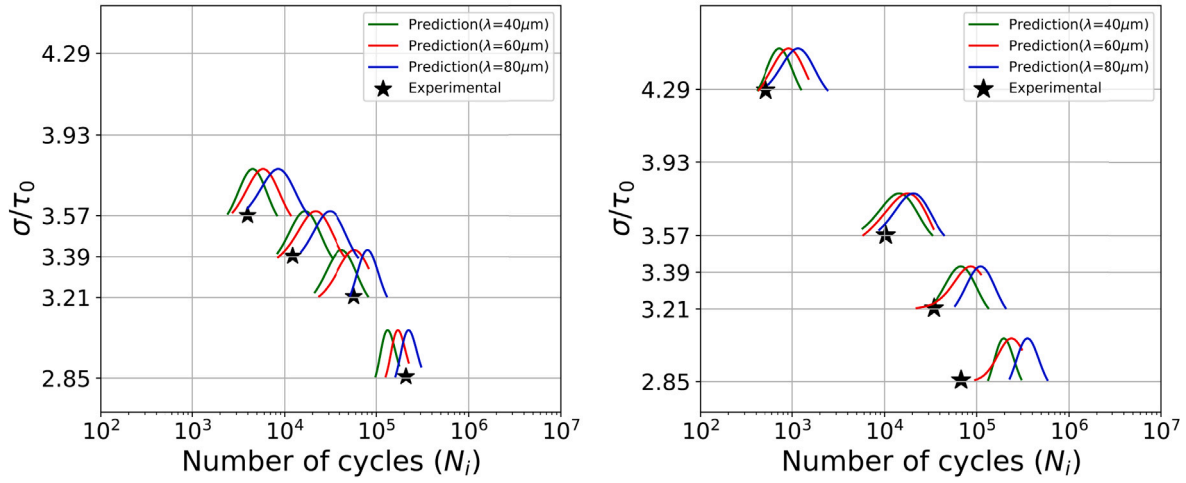

Fig. 10. The comparison of computational fatigue life for different wavelengths of surface roughness for (a) flat 1.2Z and (b) flat 1.2X samples. Please note that the black asterisk represents the experimental fatigue life at 60μm wavelength.

of roughness, uniquely described through the parameter R_a. These findings highlight the numerical interplay between surface roughness amplitude and microstructure in fatigue crack initiation.

5. Conclusions

A microstructure fatigue life prediction framework based on CPFFT is enhanced to consider the combined effect of surface roughness and polycrystalline microstructure. The approach is applied to study the fatigue performance of flat Hastelloy-X specimens produced by selective laser melting (SLM). The model considers the microstructural characteristics obtained from Electron Backscatter Diffraction (EBSD) experiments, such as grain shape, size, and orientation distributions, as well as surface roughness profiles, which are approximated as sinusoidal profiles based on actual measurements. The findings of this study demonstrate that the proposed framework is capable of accurately predicting the fatigue life of SLM-manufactured Hastelloy-X specimens.

It is shown that the model, when including explicitly the roughness profile obtain from experiments, is highly accurate in predicting the fatigue life of flat specimens using general CP and fatigue parameters of Hastelloy-X —obtained for bulk samples without roughness — without further calibration The model successfully captures the anisotropic fatigue response observed in different built orientations showing that horizontally oriented samples have a better fatigue performance than vertically oriented samples. This anisotropic behavior is thought to be due to microstructural factors such as grain shape and orientation, with no significant influence from surface roughness on the anisotropic fatigue response caused by building orientation.

After the validation of the model for the experimental parameters describing surface roughness, a parametric study was performed by systematically varying surface roughness shape. The study shows a very strong effect of the roughness amplitude R_a in stress levels and fatigue life. A translation to the right of the FIP cumulative distribution function with R_a was found for all the stress ranges considered, and life was monotonically reduced with R_a. These results are in agreement with previous research conducted by Yadollahi et al. [20], Shrestha et al. [26], and Edwards and Ramulu [58], confirming the reliability of the findings. The level of surface waviness was also varied but a minimal effect was found in stress concentration or life, confirming the validity of using only R_a to characterize the roughness experimentally.

CRediT authorship contribution statement

Chandrashekhar M. Pilgar: Writing – original draft, Visualization, Software, Methodology, Investigation, Formal analysis, Data curation. **Ana M. Fernandez:** Validation, Project administration, Methodology, Investigation, Funding acquisition. **Javier Segurado:** Writing – review & editing, Software, Methodology, Investigation, Funding acquisition, Formal analysis, Conceptualization.

Declaration of competing interest

The authors declare the following financial interests/personal relationships which may be considered as potential competing interests: Javier Segurado reports financial support was provided by Spanish ministry of Science Technology and Innovations. Chandrashekar Pilgar reports financial support was provided by Spanish ministry of Science Technology and Innovations.

Data availability

The authors do not have permission to share data.

Acknowledgments

The authors declare the following financial interests which may be considered as potential competing interests: Javier Segurado reports that financial support was provided by Spanish Ministry of Science for the project ADSORBENT, Spain, Plan estatal de I+D+i-2019: PID2019-106759GB-I00.

References

[1] Karapuzha AS, Wegener T, Krochmal M, Zhu Y, Niendorf T, Fraser D, et al. Fatigue crack growth in additively manufactured Hastelloy X - Influences of crack orientation and post-fabrication treatments. Mater Sci Eng A 2022;854:143773.
[2] Stoffregen H, Butterweck K, Abele E. Fatigue analysis in selective laser melting: Review and investigation of thin-walled actuator housings. 2014, p. 635–50.
[3] Ferrar B, Mullen L, Jones E, Stamp R, Sutcliffe C. Gas flow effects on selective laser melting (SLM) manufacturing performance. J Mater Process Technol 2012;212(2):355–64.
[4] Ali U, Mahmoodkhani Y, Shahabad SI, Esmaeilizadeh R, Liravi F, Sheydaeian E, et al. On the measurement of relative powder-bed compaction density in powder-bed additive manufacturing processes. Mater Des 2018;155:495–501.
[5] Mumtaz K, Hopkinson N. Top surface and side roughness of Inconel 625 parts processed using selective laser melting. Rapid Prototyp J 2009.

[6] Esmaeilizadeh R, Keshavarzkermani A, Faghih S, Behravesh B, Ali U, Bonakdar A, et al. Fatigue characterization and modeling of additively manufactured Hastelloy-X superalloy. J Mater Eng Perform 2022;31(8):6234–45.

[7] Abele E, Kniepkamp M. Analysis and optimisation of vertical surface roughness in micro selective laser melting. Surf Topogr Metrol Prop 2015;3(3):034007.

[8] Wang Z, Guan K, Gao M, Li X, Chen X, Zeng X. The microstructure and mechanical properties of deposited-IN718 by selective laser melting. J Alloys Compd 2012;513:518–23.

[9] Li Y, Garabedian N, Schneider J, Greiner C. Waviness affects friction and abrasive wear. Tribol Lett 2023;71(2). http://dx.doi.org/10.1007/s11249-023-01736-1.

[10] Goh CH, Wallace J, Neu R, McDowell D. Polycrystal plasticity simulations of fretting fatigue. Int J Fatigue 2001;23:423–35. http://dx.doi.org/10.1016/s0142-1123(01)00150-5.

[11] El Haddad M, Topper T, Smith K. Prediction of non propagating cracks. Eng Fract Mech 1979;11(3):573–84.

[12] Smith R, Miller K. Prediction of fatigue regimes in notched components. Int J Mech Sci 1978;20(4):201–6.

[13] Murakami Y, Endo M. Effects of hardness and crack geometries on delta k sub th of small cracks emanating from small defects. Mech Eng Publ Behav Short Fatigue Cracks 1986;275–93.

[14] Pessard E, Bellett D, Morel F, Koutiri I. A mechanistic approach to the Kitagawa–Takahashi diagram using a multiaxial probabilistic framework. Eng Fract Mech 2013;109:89–104.

[15] Le VD, Morel F, Bellett D, Saintier N, Osmond P. Simulation of the Kitagawa–Takahashi diagram using a probabilistic approach for cast Al-Si alloys under different multiaxial loads. Int J Fatigue 2016;93:109–21.

[16] Campbell R, Martorelli M, Lee H. Surface roughness visualisation for rapid prototyping models. Comput Aided Des 2002;34(10):717–25.

[17] Pérez CL, Calvet JV, Pérez MS. Geometric roughness analysis in solid free-form manufacturing processes. J Mater Process Technol 2001;119(1–3):52–7.

[18] As S, Skallerud B, Tveiten B, Holme B. Fatigue life prediction of machined components using finite element analysis of surface topography. Int J Fatigue 2005;27(10–12):1590–6.

[19] Ås SK, Skallerud B, Tveiten BW. Surface roughness characterization for fatigue life predictions using finite element analysis. Int J Fatigue 2008;30(12):2200–9.

[20] Yadollahi A, Mahtabi M, Khalili A, Doude H, Newman J. Fatigue life prediction of additively manufactured material: Effects of surface roughness, defect size, and shape. Fatigue Fract Eng Mater Struct 2018;41(7):1602–14.

[21] Vayssette B, Saintier N, Brugger C, May ME, Pessard E. Numerical modelling of surface roughness effect on the fatigue behavior of Ti-6Al-4V obtained by additive manufacturing. Int J Fatigue 2019;123:180–95.

[22] Belhadjamor M, Belghith S, Mezlini S, Mansori ME. Numerical study of normal contact stiffness: Non-Gaussian roughness and elastic–plastic behavior. Proc Inst Mech Eng 2019;234(9):1368–80.

[23] Natkowski E, Sonnweber-Ribic P, Münstermann S. Surface roughness influence in micromechanical fatigue lifetime prediction with crystal plasticity models for steel. Int J Fatigue 2022;159:106792.

[24] Pilgar CM, Fernandez AM, Segurado J. Microstructure sensitive fatigue life prediction model for SLM fabricated Hastelloy-X. Int J Fatigue 2023;168:107372.

[25] Pilgar CM, Fernandez AM, Lucarini S, Segurado J. Effect of printing direction and thickness on the mechanical behavior of SLM fabricated Hastelloy-X. Int J Plast 2022;153:103250.

[26] Shrestha R, Simsiriwong J, Shamsaei N. Fatigue behavior of additive manufactured 316L stainless steel parts: Effects of layer orientation and surface roughness. Addit Manuf 2019;28:23–38.

[27] Pegues JW, Shamsaei N, Roach MD, Williamson RS. Fatigue life estimation of additive manufactured parts in the as-built surface condition. Mater Des Process Commun 2019;1(3).

[28] Lorenz SJ, Sadeghi F, Trivedi HK, Rosado L, Kirsch MS, Wang C. A continuum damage mechanics finite element model for investigating effects of surface roughness on rolling contact fatigue. Int J Fatigue 2021;143:105986.

[29] Haouala S, Segurado J, LLorca J. An analysis of the influence of grain size on the strength of FCC polycrystals by means of computational homogenization. Acta Mater 2018;148:72–85. http://dx.doi.org/10.1016/j.actamat.2018.01.024.

[30] Haug C, Molodov D, Gumbsch P, Greiner C. Tribologically induced crystal rotation kinematics revealed by electron backscatter diffraction. Acta Mater 2022;225:117566. http://dx.doi.org/10.1016/j.actamat.2021.117566.

[31] Lindroos M, Scherer JM, Forest S, Laukkanen A, Andersson T, Vaara J, et al. Micromorphic crystal plasticity approach to damage regularization and size effects in martensitic steels. Int J Plast 2022;151:103187. http://dx.doi.org/10.1016/j.ijplas.2021.103187.

[32] Cruzado A, Llorca J, Segurado J. Modelling cyclic deformation of Inconel 718 superalloy by means of crystal plasticity and computational homogenization. Int J Solids Struct 2017;122(123):148–61.

[33] Tome C, Canova G, Kocks U, Christodoulou N, Jonas J. The relation between macroscopic and microscopic strain hardening in FCC polycrystals. Acta Metall 1984;32(10).

[34] Lucarini S, Segurado J. On the accuracy of spectral solvers for micromechanics based fatigue modeling. Comput Mech 2018;63(2):365–82.

[35] Lucarini S, Upadhyay MV, Segurado J. FFT based approaches in micromechanics: fundamentals, methods and applications. Modelling Simul Mater Sci Eng 2021;30(2):023002.

[36] Vondřejc J, Zeman J, Marek I. An FFT-based Galerkin method for homogenization of periodic media. Comput Math Appl 2014;68(3):156–73.

[37] de Geus TWJ, Vondřejc J, Zeman J, Peerlings RHJ, Geers MGD. Finite strain FFT-based non-linear solvers made simple. Comput Methods Appl Mech Engrg 2017;318:412–30.

[38] Willot F, Abdalla B, Pellegrini Y. Fourier-based schemes with modified green operator for computing the electrical response of heterogeneous media with accurate local fields. Internat J Numer Methods Engrg 2014;98(7):518–33.

[39] Lucarini S, Segurado J. An algorithm for stress and mixed control in Galerkin-based FFT homogenization. Internat J Numer Methods Engrg 2019;119(8):797–805.

[40] Manonukul A, Dunne FPE. High– and low–cycle fatigue crack initiation using polycrystal plasticity. Proc R Soc Lond A Math Phys Eng Sci 2004;460(2047):1881–903.

[41] Sweeney CA, Vorster W, Leen SB, Sakurada E, McHugh PE, Dunne FPE. The role of elastic anisotropy, length scale and crystallographic slip in fatigue crack nucleation. J Mech Phys Solids 2013;61:1224–40.

[42] McDowell D, Dunne F. Microstructure-sensitive computational modeling of fatigue crack formation. Int J Fatigue 2010;32(9):1521–42.

[43] McDowell D, Gall K, Horstemeyer M, Fan J. Microstructure-based fatigue modeling of cast A356-T6 alloy. Eng Fract Mech 2003;70(1):49–80.

[44] Sweeney C, McHugh P, McGarry J, Leen S. Micromechanical methodology for fatigue in cardiovascular stents. Int J Fatigue 2012;44:202–16.

[45] Sweeney C, O'Brien B, McHugh P, Leen S. Experimental charactrisation for micromechanical modelling of CoCr stent fatigue. Biomaterials 2014;35:36–48.

[46] Bennett V, McDowell D. Polycrystal orientation distribution effects on microslip in high cycle fatigue. Int J Fatigue 2003;25(1):27–39.

[47] Castelluccio GM, McDowell DL. Mesoscale modeling of microstructurally small fatigue cracks in metallic polycrystals. Mater Sci Eng A 2014;598:34–55.

[48] Wan V, MacLachlan D, Dunne F. A stored energy criterion for fatigue crack nucleation in polycrystals. Int J Fatigue 2014;68:90–102. http://dx.doi.org/10.1016/j.ijfatigue.2014.06.001, URL: https://www.sciencedirect.com/science/article/pii/S0142112314001625.

[49] Sweeney C, O'Brien B, Dunne F, McHugh P, Leen S. Micro-scale testing and micromechanical modelling for high cycle fatigue of CoCr stent material. J Mech Behav Biomed Mater 2015;46:244–60.

[50] Dunne F. Fatigue crack nucleation: Mechanistic modelling across the length scales. Curr Opin Solid State Mater Sci 2014;18.

[51] Ozturk D, Shahba A, Ghosh S. Crystal plasticity FE study of the effect of thermo-mechanical loading on fatigue crack nucleation in titanium alloys. Fatigue Fract Eng Mater Struct 2016;39:752–69.

[52] Sangid MD. The physics of fatigue crack initiation. Int J Fatigue 2013;57:58–72.

[53] Guerchais R, Robert C, Morel F, Saintier N. Micromechanical study of the loading path effect in high cycle fatigue. Int J Fatigue 2014;59:64–75. http://dx.doi.org/10.1016/j.ijfatigue.2013.09.014, URL: https://www.sciencedirect.com/science/article/pii/S0142112313002752.

[54] Rovinelli A, Guilhem Y, Proudhon H, Lebensohn RA, Ludwig W, Sangid MD. Assessing reliability of fatigue indicator parameters for small crack growth via a probabilistic framework. Modelling Simul Mater Sci Eng 2017;25(4):045010. http://dx.doi.org/10.1088/1361-651X/aa6c45.

[55] McDowell D, Dunne F. Microstructure-sensitive computational modeling of fatigue crack formation. Int J Fatigue 2010;32(9):1521–42.

[56] Jiang D, Tian Y, Zhu Y, Huang A. Investigation of surface roughness post-processing of additively manufactured nickel-based superalloy Hastelloy X using electropolishing. Surf Coat Technol 2022;441:128529. http://dx.doi.org/10.1016/j.surfcoat.2022.128529, URL: https://www.sciencedirect.com/science/article/pii/S0257897222004509.

[57] Sanaei N, Fatemi A. Analysis of the effect of surface roughness on fatigue performance of powder bed fusion additive manufactured metals. Theor Appl Fract Mech 2020;108:102638. http://dx.doi.org/10.1016/j.tafmec.2020.102638, URL: https://www.sciencedirect.com/science/article/pii/S0167844220302147.

[58] Edwards P, Ramulu M. Fatigue performance evaluation of selective laser melted Ti–6Al–4V. Mater Sci Eng A 2014;598:327–37.